Microstructure-texture-micro-strain evolution during tensile deformation of α+β titanium alloy using in-situ Synchrotron X-ray diffraction and CPFEM simulation

Microstructure-texture-micro-strain evolution during tensile deformation of α+β titanium alloy using in-situ Synchrotron X-ray diffraction and CPFEM simulation

Atasi Ghosh[1,4], **Roopam Jain**[1], **Heinz-Guenther Brokmeier**[2,3], **Nilesh Gurao**[1]

[1]Department of Materials Science and Engineering, IIT Kanpur, Kalyanpur, Kanpur, Uttar Pradesh-208016, India
[2]Institute of Materials Science and Engineering, Clausthal University of Technology, Agricollastaβe 6, D-38678, Clausthal-Zellerfeld, Germany
[3]Helmholtz-Zentrum Geesthacht Max Planck Staβe 1, D-21502, Geesthacht, Germany

[4]Corresponding author's e-mail id: atasig@gmail.com

Abstract. The evolution of micro-strain and crystallographic texture of each phase of α+β Ti-6Al-4V titanium alloy generated during tensile deformation has been estimated numerically and then compared with the experimental results. It has been carried out based on the Crystal Plasticity Finite Element Model (CPFEM) simulation of the stress-strain curve till the uniform elongation for the equiaxed microstructure is generated synthetically. The synthetic microstructure of Ti-6Al-4V has been developed using the microstructure feature parameters (such as grain size, phase fraction, and grain orientation). The polycrystal stress-strain behaviour for the same has been simulated using the representative orientation distribution function data obtained from the electron backscatter diffraction (EBSD) scans. The present investigation discusses the mechanism of strain-partitioning during uniform elongation using CPFEM simulation in conjunction with EBSD-based experimental misorientation data to rationalize our observation.

1. Introduction

The phenomenon of strain partitioning is a well-established mechanism of deformation observed in the two-phase microstructure. The strain partitioning in the lamellar microstructure of martensite/ferrite phase of dual-phase steel [1-2], ferrite/cementite in pearlitic steel [3], and austenite/martensite in Mn steel [4] have been studied experimentally using in-situ synchrotron X-ray diffraction and in-situ Digital Image Correlation (DIC) techniques, respectively. Moreover, the role of strain-partitioning in the deformation behaviour has been rationalized using Elasto-Plastic-Self-Consistent (EPSC) numerical simulation for the Ti-6Al-4V alloy with bimodal microstructure [5]. However, a homogeneous macroscopic plasticity model could not simulate the plastic deformation behaviour of two-phase heterogeneous microstructures successfully. Earlier researchers have developed improved semi-automated stereological methodologies [6] to measure the microstructural feature parameters and predict the mechanical property based on the Bayesian neural network model [7] with some extent of accuracy. Such a model is primarily based on the statistical and geometrical aspects of the microstructural features and does not include crystallographic texture. It is very difficult to obtain information regarding the

deformation strain of individual phases experimentally due to strong interdependencies between microstructural variables. Hence, a multi-scale simulation model based on both the dimensional and textural aspects of microstructure for the plasticity analysis is warranted.

An alternative approach is to create digital 3D microstructures that are a statistical distribution of microstructural features within a real material of interest and simulate their stress-strain behaviour. The Crystal Plasticity Finite element method (CPFEM) is a microstructure scale-based model which captures the effect of grain orientation, complex visco-plastic deformation behaviour, and the length scale effects of some key microstructural features. The amount of lattice misorientation during deformation gives an indirect measure of slip activity and could be easily measured using Electron backscatter diffraction (EBSD). However, in the present era of near net shape component design through additive manufacturing techniques, it is not always possible to determine the mechanical property experimentally. Therefore, it has become extremely important to develop predictive models and validate them for different simple and complex microstructures. Ti-6Al-4V is a two-phase alloy and is a candidate material for additive manufacturing for aerospace applications. Hence, in the present study, the correlation between the micro-strain partitioning and micro-texture evolution of individual phases during tensile deformation of Ti-6Al-4V has been established using a combinatorial approach.

2. Experimental Methods

2.1. Material

The present investigation was carried out on the hot-rolled plate of Ti-6Al-4V alloy obtained from the Defence Metallurgical Research Laboratory (DMRL), Hyderabad. The microstructure of the as-received plate consists of fine equiaxed grains of alpha (hcp, grey) with beta (bcc, white) phase as isolated particles distributed at the grain boundaries as shown in the low magnification optical image and from the high magnification secondary electron image using Scanning Electron Microscope (SEM) in figure 1a and figure 1b, respectively. The schematic representation of the pole figure map of the ideal orientation relation ($(0002)\alpha||(011)\beta$ and $[11\bar{2}0]\alpha||[111]\beta$) between the alpha and the beta phase has been shown in figure 1c.

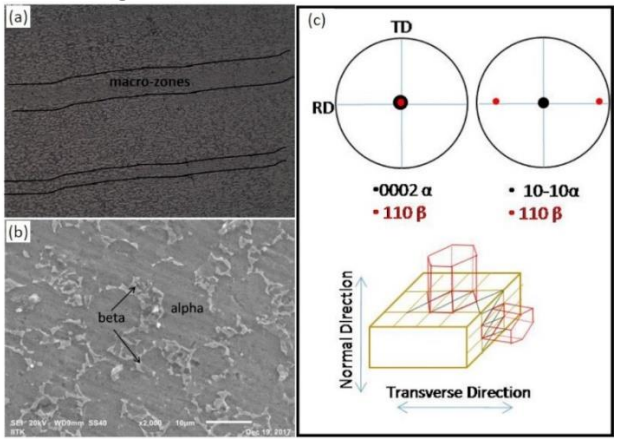

Figure 1. Alpha and beta phase morphology shown in a) optical micrograph, b) SEM micrograph and c) schematic representation of macro-texture.

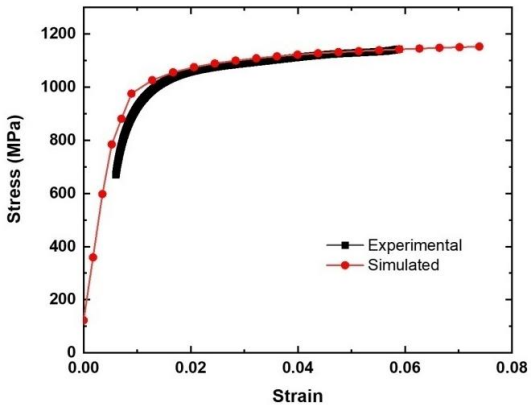

Figure 2. Experimental stress-strain curve simulated using CPFEM.

2.2. Tensile testing

In-situ and ex-situ tensile tests have been carried out till fracture. Tensile specimens of Ti-6Al-4V alloy with the loading axis oriented along the rolling direction have been machined out by an Electrical discharge machine (EDM). The in-situ tensile testing has been carried out using a screw-driven tensile testing stage aligned with the Synchrotron X-ray source in Desy lab, Germany. The ex-situ tensile testing has been carried out using the servo-electric Universal Tensile Testing Machine of INSTRON.

2.3. In-situ synchrotron X-ray texture measurement

In-situ synchrotron X-ray diffraction was carried out to measure texture at loads of 0 kN, 2 kN, and 6 kN during tensile deformation. After tensile failure texture has been measured at 1mm away from the fracture tip and near the fracture region of the fractured specimen. PETRA III beamline P07 with the energy of 6.033 GeV machine was used to measure deformation texture exactly in the middle of the gauge section of the tensile specimen during tensile deformation in transmission geometry. A beamline called HEMS P07B of Wavelength 0.143155 Å and energy of 87 keV was used. The Debye-Scherrer rings obtained have been converted to an intensity peak profile using Fit2D software [8] and were used to calculate the crystallite size, micro-strain, and dislocation density. The output of Fit2D was the input for texture calculation software Resmat [9]. The data were used for the construction of the 3D-Orientation Distribution Function, and pole figures.

2.4. Electron backscatter diffraction

For the post-deformation microstructure and micro-texture samples were prepared from the gauge section of the tensile test specimens. An area of 100 x 100 μm^2 was scanned at step sizes of 0.25 µm exactly in the middle of the gauge portion of the tensile specimen where Synchrotron diffraction was carried out in JEOL FESEM. Crystal orientation and Kernel Average Misorientation (KAM) maps were generated using TSL software.

2.5. Synthetic microstructure

From the initial micrograph shown in figure 1b, it is apparent that the very fine grains of the beta phase is distributed at the grain boundaries of the large equiaxed alpha phase. To generate such a microstructure numerically, a separate cluster of beta phase (~2.30±0.4 µ) has been generated and then distributed along the grain boundaries of equiaxed randomly oriented alpha phase (~243±5 µ) microstructure maintaining the volume fraction of beta as ~8%. Synthetic microstructures were generated using the open-source Dream.3D software [10].

2.6. Simulation procedure

The simulated true stress-true strain curve has been obtained using crystal plasticity simulation. Beta phase deformation in Ti-6Al-4V is observed only at high strain (near fracture) or at high temperatures and hence ignored. The crystal plasticity simulation procedure has been adopted from the following ref. [11-12]. The applied stress tensor $\sigma(x)$ is directly related to the slip rate of the s slip system by Eq. 1.

$$\dot{\gamma^s}(x) = \dot{\gamma_0}\left(\frac{|m^s(x):\sigma(x)|}{\tau_0^s}\right)^n sgn\left(m^s(x):\sigma(x)\right) \quad (1)$$

$\dot{\gamma^s}$ is the shear strain rate on s slip system, $\dot{\gamma_0}$ is the reference plastic shear rate, $m^s(x)$ is the Schmid tensor of s slip system, τ_0^s is the critical resolved shear stress for slip system s and n is the inverse of the strain rate sensitivity. The plastic strain rate tensor $\dot{\varepsilon}^p$ from multiple slips is given by Eq. 2.

$$\dot{\varepsilon}^p = \sum_{s=1}^{N} m^s(x)\,\dot{\gamma^s}(x) \quad (2)$$

For titanium alloy with low strain hardening, the critical resolved shear stress has been kept constant throughout the simulation and the elastic constants are given in Table 1.

Table 1. Material Parameters used for the simulations

Parameter	C11	C12	C13	C33	C44	τ_0^{basal}	$\tau_0^{prismatic}$	$\tau_0^{pyramidal}$
value	162 GPa	92 GPa	69 GPa	180 GPa	46 GPa	338 MPa	352 MPa	700 MPa

3. Results

3.1. Macro-scale and micro-scale tensile response

The polycrystal stress-strain behaviour simulated using the CPFEM homogenization scheme matches well with the experimentally determined macro-scale stress-strain response, shown in figure 2. The yield

strength, ultimate tensile strength, and percent uniform elongation have been reported in Table 2. The tensile stress-strain behaviour of Ti-6Al-4V closely resembles that of the elastic-perfectly plastic nature with a low strain hardening rate.

Table 2. Mechanical property of Ti-6Al-4V alloy

Yield strength (MPa)	Tensile Strength (MPa)	Young's Modulus (GPa)	Elongation (%)
850.58	929.52	107.29	7.5

3.2. Micro-strain and dislocation density

The variation of micro-strain and dislocation density of both alpha and beta phases as a function of grain orientation and load determined from the synchrotron X-ray diffraction line profile analysis using the pseudo-variance method has been shown in figure 3. The $(10\bar{1}0)$ oriented alpha grains show a significant increase in micro-strain and dislocation density which is expected as the <0002> direction is parallel to the applied load axis, however, the increase in the dislocation density of (110) oriented beta grains with less increase in micro-strain could be interpreted from the deformation behaviour of ultra-fine grain size according to the Hall-Petch relation. The beta phase can accommodate more dislocations because of the more open structure of the bcc phase. It indicates that the ultrafine bcc beta phase acts as a harder phase compared to the large-grained hcp alpha phase.

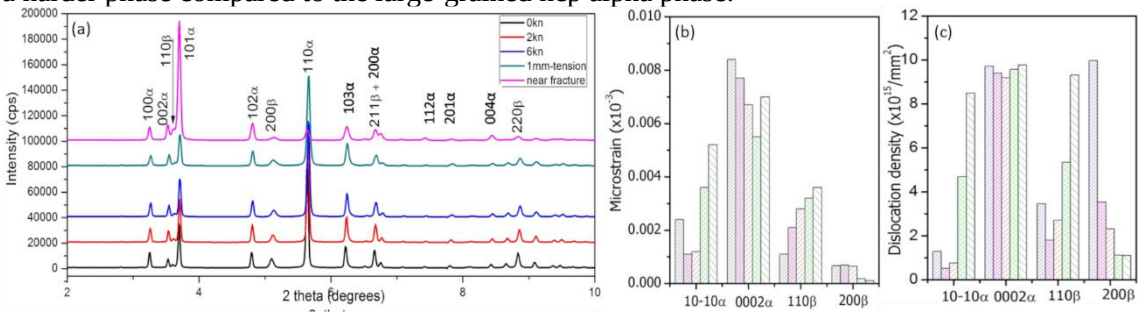

Figure 3. a) Synchrotron X-ray diffraction profile, b) Micro-strain, and c) Dislocation density

3.3. Deformation texture

The pole figure maps shown in figure 4a depict that at low load the prism poles show more rotation as compared to the basal pole and with the increase in load and near the fracture region basal pole rotation is significant. After deformation the beta phase texture changes from the rotated cube texture to the Goss texture. Another interesting observation is that the rotation of the 110 poles of the beta phase has occurred in the opposite direction to that of the basal pole which could be due to cross slip as shown schematically in figure 4b. Thus, the partial orientation relationship of $(0002)\alpha \| (110)\beta$ present initially is completely lost after tensile deformation.

3.4. Crystal orientation and Kernel Average Misorientation map

The deformation microstructure, micro-texture, and local misorientation of the alpha and beta phases were obtained using an EBSD scan close to the fracture tip shown in figure 5a. The corresponding simulated maps for 3% and 6% strain has been shown in figure 5b. It indicates that at lower strain (3%) the micro-texture variation within the prism (blue) grains is higher compared to the basal (red) or near basal (yellow, orange) oriented grains. Hence, the low KAM value of basal-oriented grains has been observed. However, at higher strain (6%), the basal grains are highly fragmented and the misorientation value has increased within the small fragments of basal grains while the prism-oriented grains have a low KAM value. It shows a good match between the experimental near fracture and simulated 6% strain maps. The experimental crystal orientation map also shows very few pyramidal grains having tensile twins as twinning is not a dominant mode of deformation in Ti-6Al-4V, unlike Ti or Mg. Very interestingly the twin grain boundaries show a low KAM value. However, the simulated maps could not

predict twinning and no grain deformation information of the beta phase at the microstructural level of characterization could be revealed because of its ultrafine grain size.

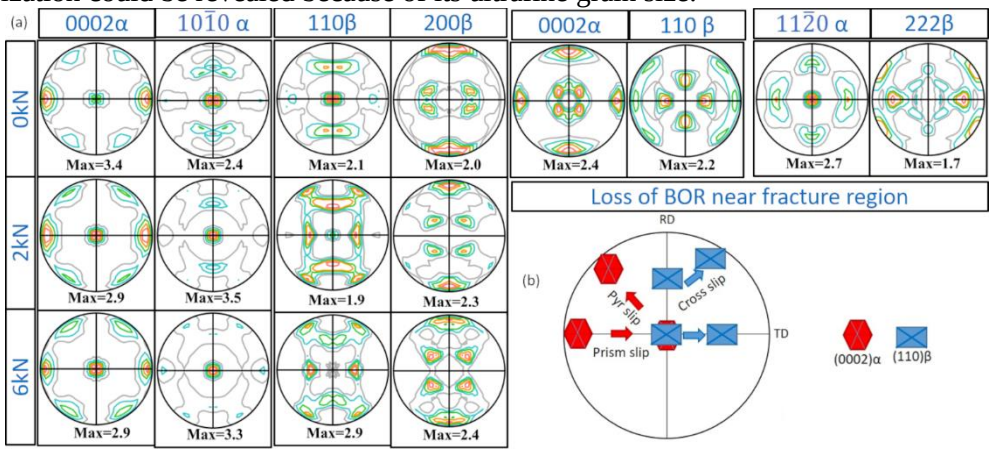

Figure 4. a) Evolution of deformation texture during tensile deformation b) Schematic representation of deformation pole figure.

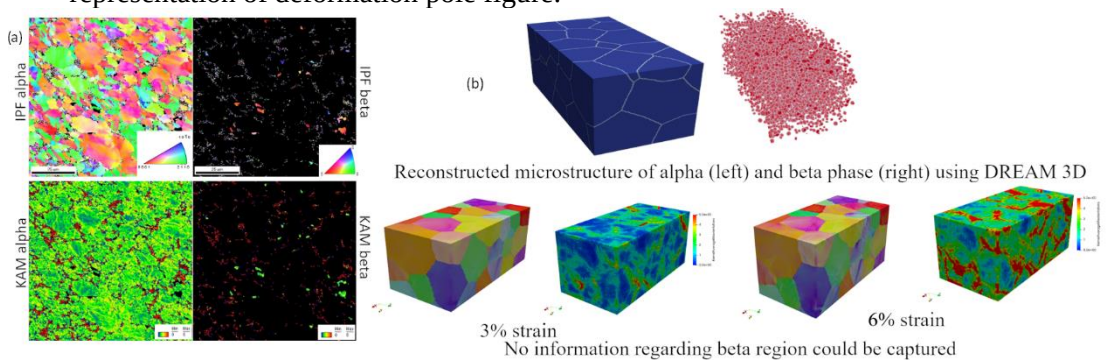

Figure 5. Crystal orientation and Kernel Average Misorientation map of Ti-6Al-4V a) experimental and b) simulated.

4. Discussion

4.1. Strain partitioning during tensile deformation

The microstructural integrity during the deformation of polycrystalline material is maintained by the mutual interference of the strain fields of dislocations within the constituent single-crystal structures. The microstructure of equiaxed alpha/beta Ti-6Al-4V can be visualized from the alpha phase or beta phase point of view. In Ti-6Al-4V, alpha phase deformation is mainly accommodated by <c+a> pyramidal slip due to the extension of the c-axis up to a certain limit without any deformation along the a-direction, and twinning is suppressed in Ti-6Al-4V. The basal-oriented grain being elastically hard will accommodate more stress and will be plastically less strained and hence will have less influence on the plastic deformation of the neighbouring grains [13].

On the other hand, the microstructure consists of macrozones of prism-pyramidal oriented grains. Such orientations being favourably oriented for basal slip exhibits easy slip transition. The slip transition mechanism operative could be visualized as the cumulative effect of the micro-scale structural features such as the shape, size, morphology, and the initial orientation of the grains in polycrystals as opposed to dislocation structure in single crystals. These slip transfer effects are widespread and are not specific to localized regions in the microstructure. The deformation features observed under Transmission Electron Microscope (TEM) foils and Electron backscatter diffraction (EBSD) scans alone cannot capture the widespread effect on the microstructure to dominate the micro-mechanical response because of their respective limitations. Multi-scale crystal plasticity simulation proved to be effective for the same.

4.2. Role of ultrafine beta phase

In alpha/beta titanium alloy, the alpha phase nucleated on the beta matrix maintains an orientation relationship with the beta matrix. There are twelve variants of alpha phase possible, however, the number of possible variants depend on beta grain boundary characteristic, thus, enhancing the nucleation of certain specific orientations and suppressing the remaining variants. For an equiaxed microstructure single variant alpha grows out of the beta matrix. Crystallographic texture results indicate the Burgers orientation relationship is not maintained in the region close to the fracture region of the tensile specimen. It is mainly due to the unique dislocation reaction specific to the alpha/beta dislocation area [14]. The primary reason for this could be the beta phase is not a close-packed crystal structure, and can accommodate Geometrically Necessary Dislocations (GNDs) to maintain compatibility with the neighbouring grains, and the orientation relationship with the alpha phase is lost during the process. Moreover, the beta phase can accommodate screw dislocations well, thus making the alpha/beta interphase boundary behave as a twist boundary. Therefore, the ultrafine beta grain appears to provide a lubricating action between the neighbouring alpha grains which reduces the flow stress and hence low strain hardening rate.

5. Conclusions

The present investigation led to the following conclusions:

- The micro-strain produced during tensile deformation is accommodated primarily in the prism-oriented alpha phase. A good match between the experimental and simulated KAM values was found to be high at the grain boundaries before fracture.
- The evolution of deformation micro-texture leads to the loss of Burgers orientation relation $(0002)\alpha \| (110)\beta$ via the rotation of the $(0002)\alpha$ grains in the direction opposite to that of $(110)\beta$ grains in the crystallographic space. CPFEM simulation fails to predict such behaviour.

Acknowledgments

The authors would like to thank Dr. Reshma Sonkusare for her help in carrying out experiments in the synchrotron X-ray diffraction facility in DESY (Deutsches Elektronen-Synchrotron) lab in Hamburg, Germany.

References

[1] Ghadbeigi H *et al* 2010 *Mater. Sci. Eng. A* **527** 5026-32.
[2] Park K *et al* 2014 *Mater. Sci. Eng. A* **604** 135-41
[3] Gadalinska E *et al* 2020 *Int. J. of Plasticity* **127** 102651.
[4] Dutta A *et al* 2019 *Materialia* **5** 100252.
[5] Chong Y *et al* 2019 *J Alloys and Compds* **811** 152040.
[6] Collins P C *et al* 2009 *Mater. Sci. Eng. A* **508** 174-82.
[7] Kar S K *et al* 2006 *Metall. Mater. Trans. A* **37A** 559-66.
[8] Hammersley H, The FIT2D Home Page**,** http://www.esrf.eu/computing/scientific/FIT2D/ (1999)
[9] TexTools Software, Resmat Corporation, Montreal, QC, Canada (2016)
[10] Groeber M A *et al* 2014 *Integr. Mater. Manuf. Innov* **3** 56-72.
[11] Lebensohn R A *et al* 2012 *Int. J. Plasticity* **32-33** 59-69.
[12] Hémery S *et al* 2019 *Acta Materialia* **181** 36-48.
[13] Banerjee D *et al* 2013 *Acta Mater.* **61** 844-79.
[14] Gungor MN *et al* 2005 Mater. Sci. Eng. A **410-411** 369-74.